Figuring Out a Complicated World

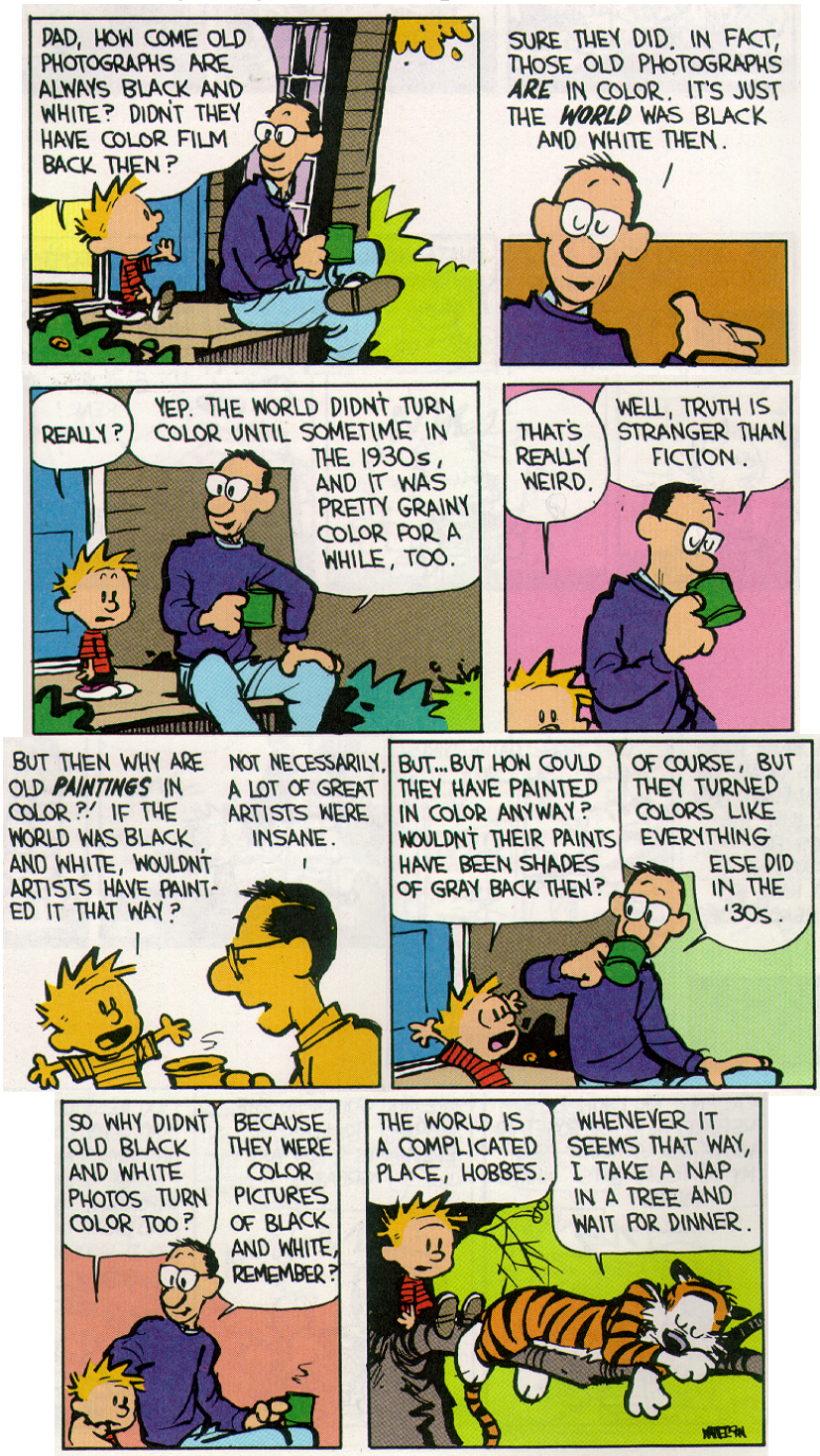

I have felt like taking many naps during the last seven years. Fortunately I didn't.

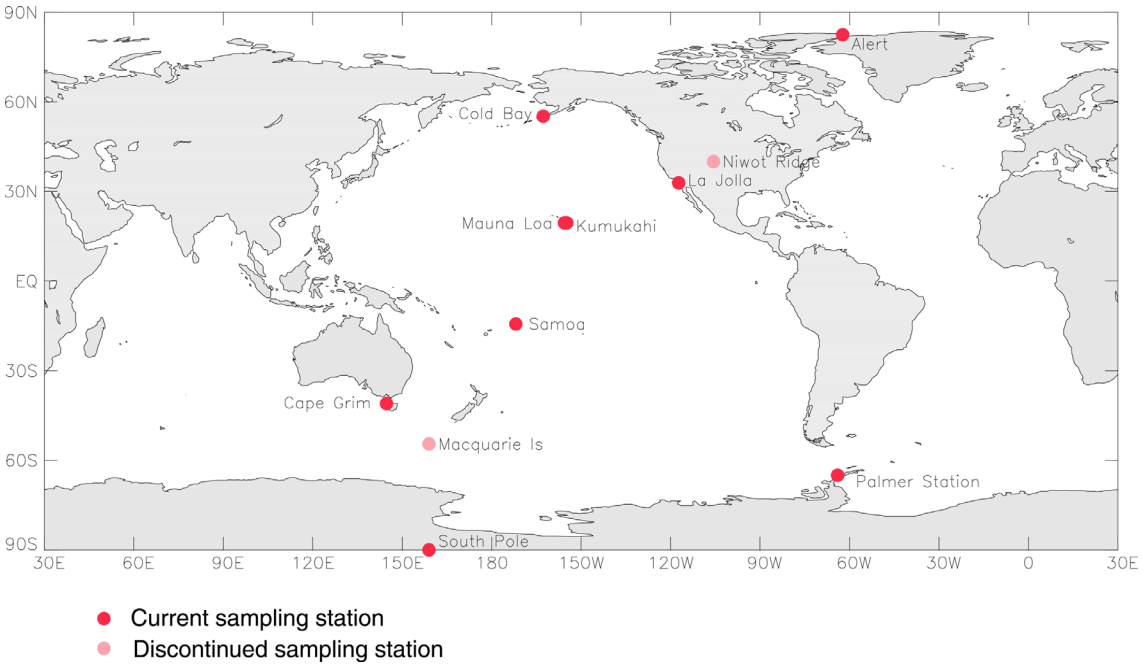

Figure 2.1. Map showing the locations of the eleven sampling stations in the Scripps O_2/N_2 network as listed in Table 2.1. Mauna Loa (MLO) and Cape Kumukahi (KUM) are shown as one point. Niwot Ridge (NWR) and Macquarie Island (MCQ) stations have now been discontinued. With the exceptions of Niwot Ridge (3749 m), Mauna Loa (3397 m) and South Pole (2810 m), all stations are approximately at sea level and coastal and therefore they are situated in the marine boundary layer.

available, relatively steady, non-fluctuating, *in situ* atmospheric CO_2 concentrations, or criteria based on other trace gas species which are measured *in situ*. We wish to sample air that has not been contaminated by local or regional anthropogenic or terrestrial processes.

In this manner we can observe synoptic and hemispheric-scale spatial trends, and seasonal and interannual temporal trends. Thus, for example, stations such as La Jolla (LJO) and Cape Grim (CGO), require a relatively narrow wind direction window (roughly westerlies for both stations) to meet these sampling requirements. Cape

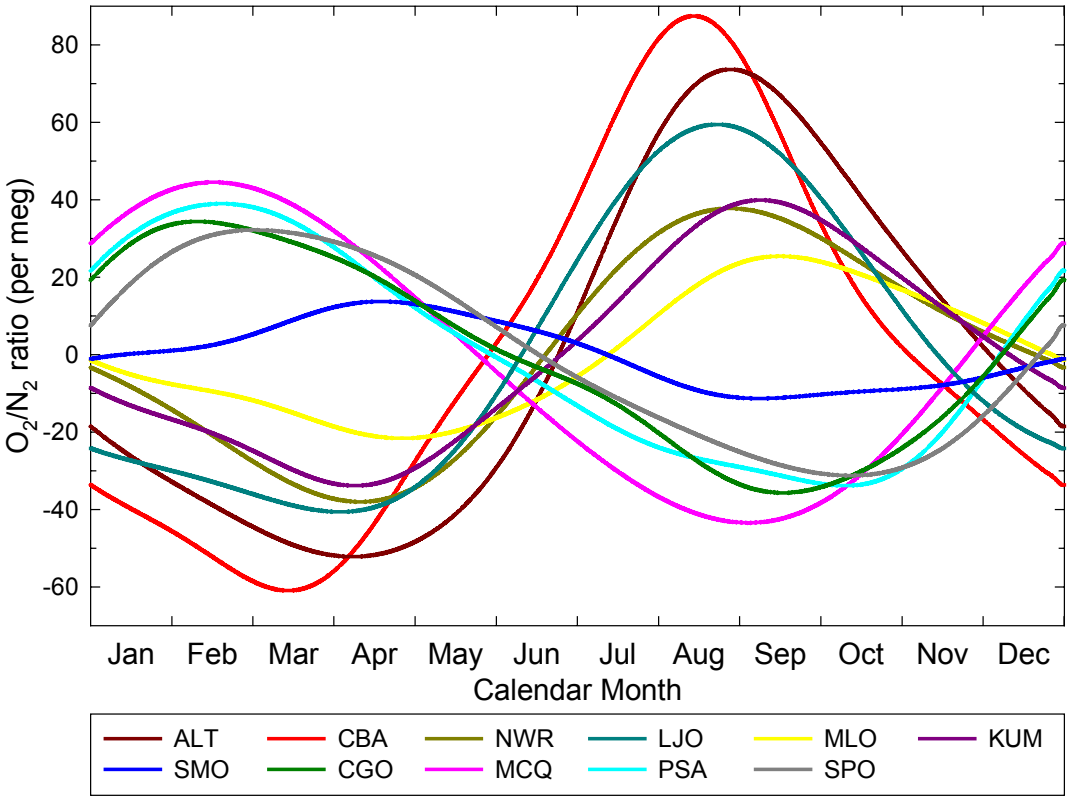

Figure 2.6. Shows the seasonal cycle component of the curve fits from Figure 2.2 for O_2/N_2 ratios for all stations, after correcting data as described in Section 2.2.3. Amplitude and phasing variations can be compared between different stations in this figure.

independent O_2/N_2 sampling program at Point Barrow, Alaska (71°19'N, 156°36'W), also in close proximity to the Bering Sea, where similar large seasonal amplitudes are observed (M. Bender, personal communication).

Cold Bay also shows a significantly earlier minimum in both O_2/N_2 ratios and APO and a slightly earlier maximum in CO_2 than other northern hemisphere stations (Figures 2.6, 2.7, and 2.8), indicating an earlier start of the "spring thaw" in both the marine and land biota. Alert exhibits the latest start in the spring thaw, as could be

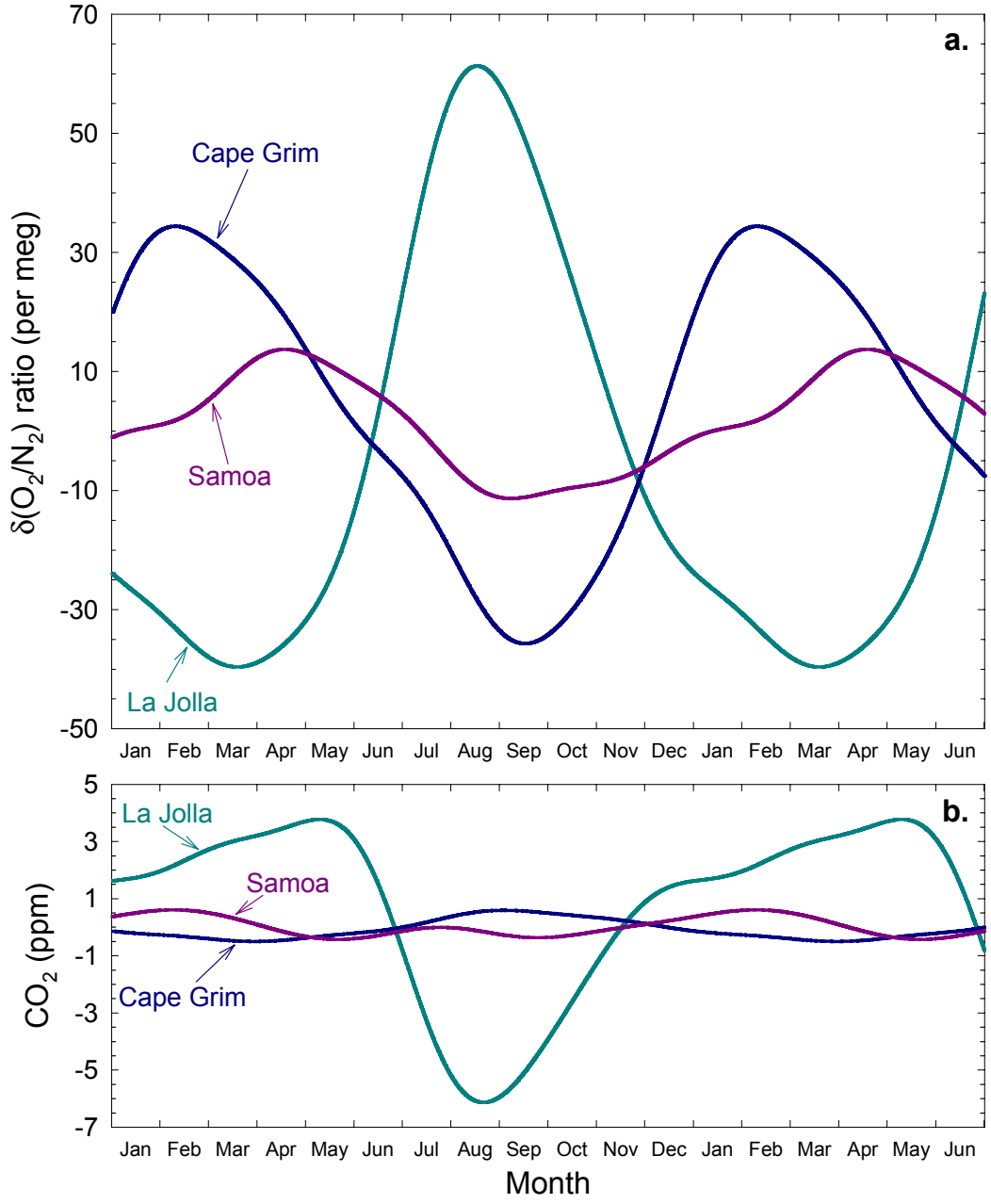

Figure 2.9. Four-harmonic seasonal components of the Samoa curve fits in Figures 2.2 and 2.3, showing O_2/N_2 ratios (a) and CO_2 concentrations (b). Also shown for comparison are similar seasonal curve fits calculated from Cape Grim and La Jolla, representing the mid-latitudes of the southern and northern hemisphere respectively. To show the seasonal characteristics more clearly, the first six months of each cycle are repeated. Southern hemisphere and northern hemisphere cycles are roughly six months out of phase with each other, whereas Samoa shows a more complicated signal. Plots a and b have been scaled so that changes in O_2 and CO_2 can be compared visually on a mole to mole basis.

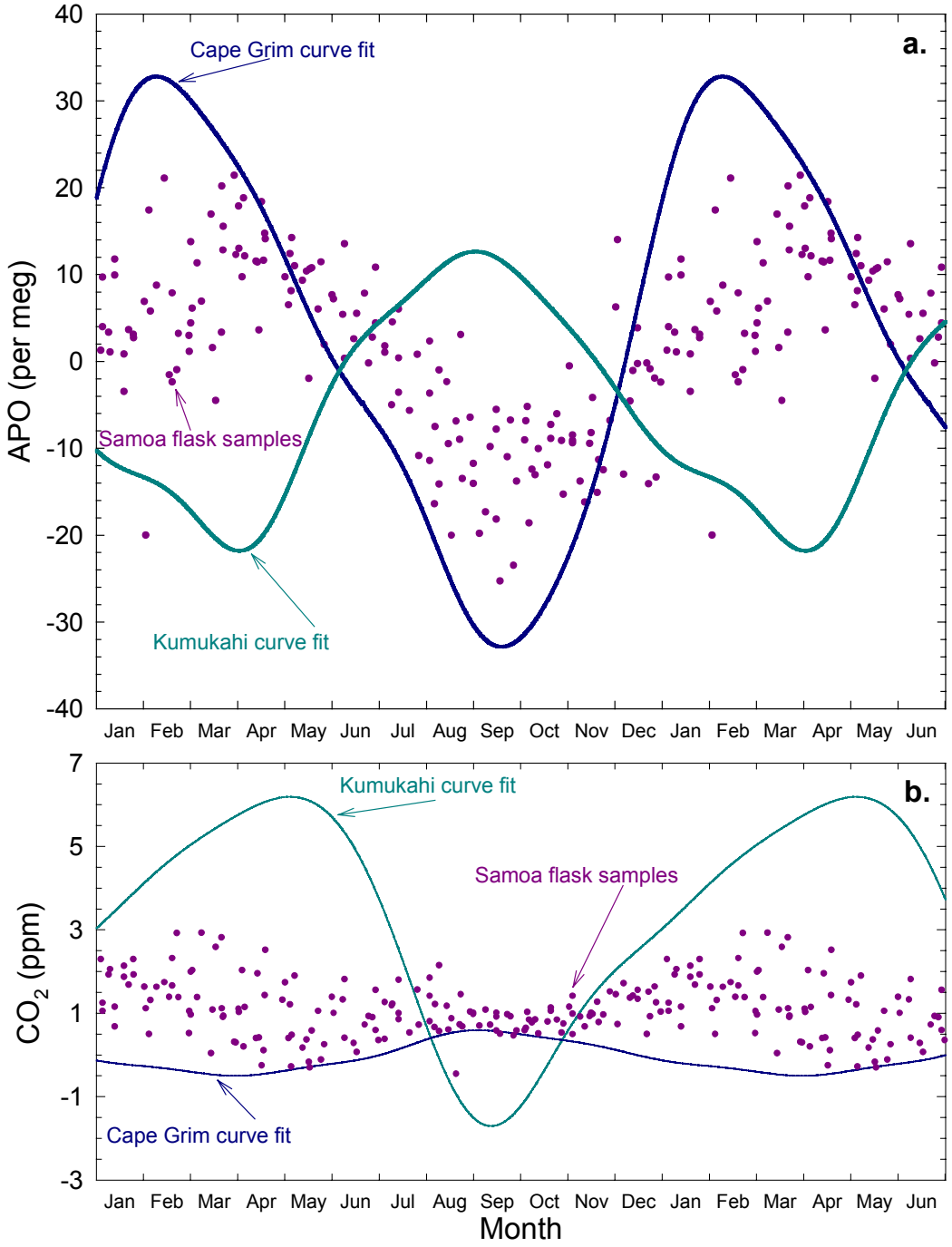

Figure 2.12. Shows oceanic (a) and land biotic (b) influences on the air masses arriving at Samoa. Atmospheric Potential Oxygen (APO), defined in the text (section 2.2.2), is essentially not influenced by land biotic processes and therefore represents oceanic influences. The seasonal component of the Samoa flask samples are shown, as well as seasonal curve fits from Cape Grim and Cape Kumukahi, representing the nearest stations from which I have data in the southern and northern hemisphere respectively. Data have been normalized as described in the text. As with Figure 2.9, the first six months of each cycle are repeated, and the plots have been scaled to be able to visually compare mole to mole changes in APO and CO_2 concentrations.

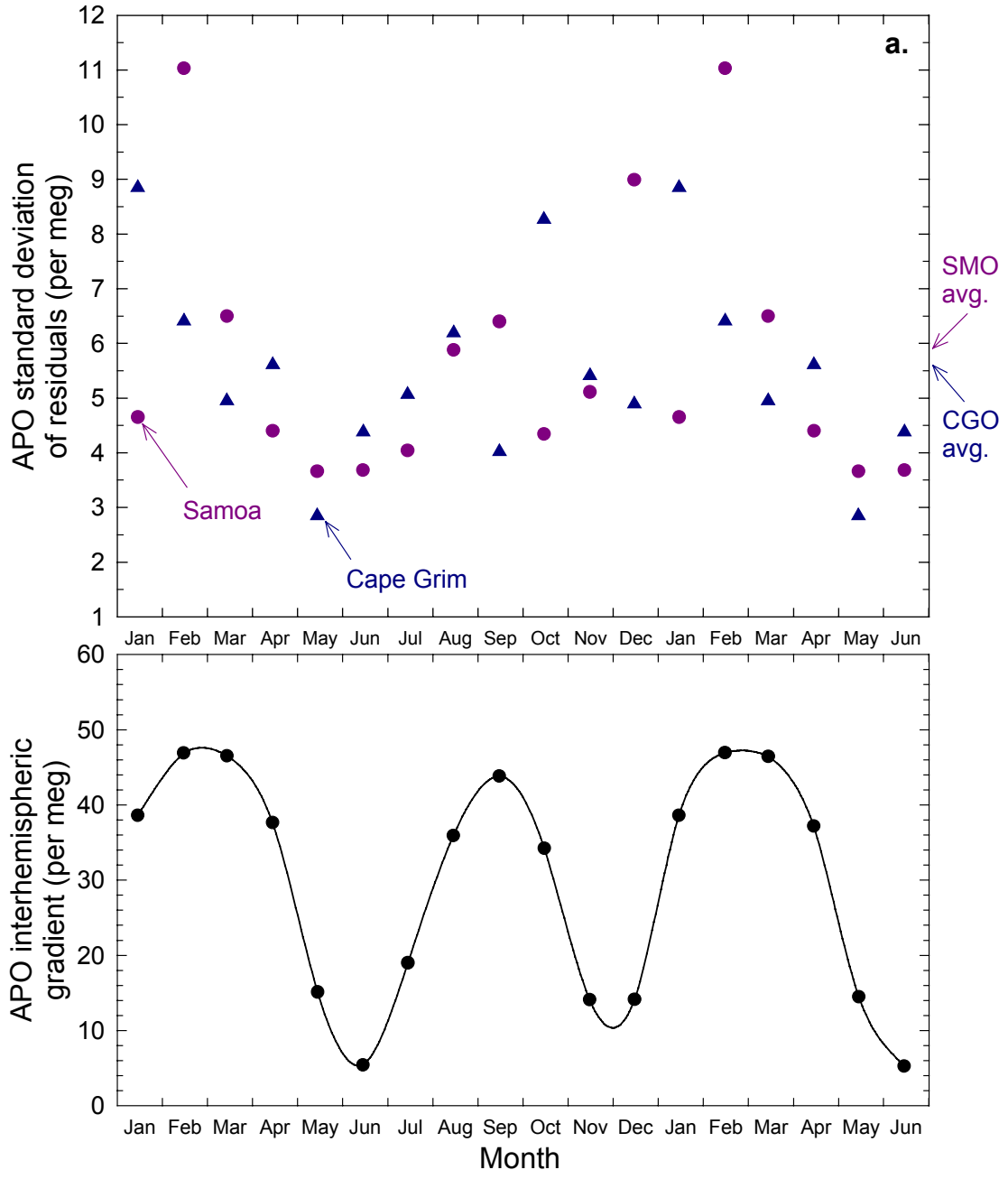

Figure 2.13a. The top plot shows APO monthly standard deviations of the residuals of the flask data from Figure 2.4 from the curve fits in the same figure. Results are shown for both Samoa and Cape Grim, and the first six months are repeated. The annual average residual at each station is indicated on the right. There is little to distinguish between Samoa and Cape Grim, and there is only weak evidence of a seasonal trend in the residuals at both stations. The bottom plot shows the absolute magnitude of the north-south interhemispheric gradient, calculated each month, and using Cape Grim and Cape Kumukahi data as representative of the southern and northern hemisphere respectively to calculate the gradient.

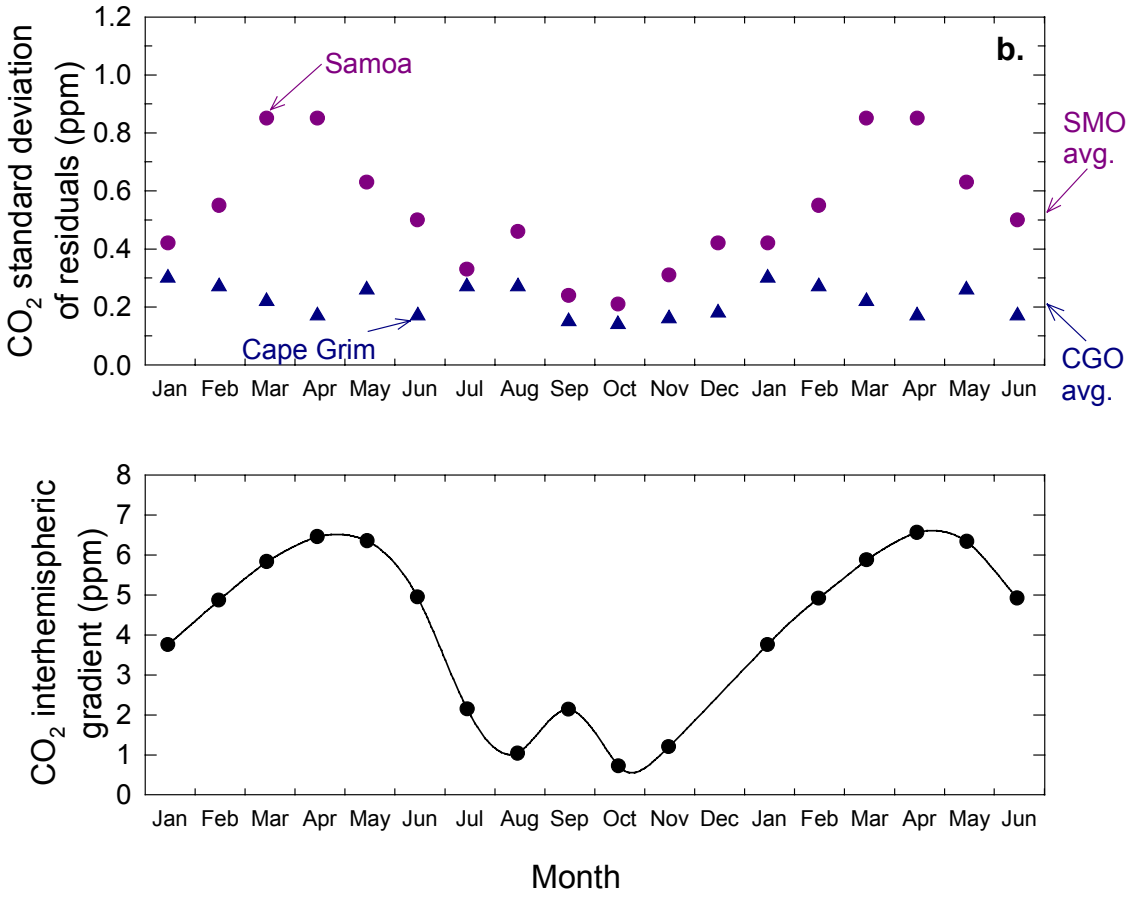

Figure 2.13b. Top and bottom plots as for Figure 2.13a, except showing CO_2 concentration. As for Figures 2.9 and 2.12, APO and CO_2 changes are visually comparable between Figures 2.13a and b. In contrast to APO, CO_2 shows a clear seasonal pattern in variability at Samoa, indicated here with higher standard deviations, whereas Cape Grim does not appear to show any seasonality. The pattern at Samoa appears to correlate well with the north-south interhemispheric gradient. Contrasting the magnitude of APO variability with CO_2, it can be seen that the APO signal is much "noisier", reflecting the presence of larger sources and sinks for O_2 in the southern hemisphere compared to CO_2.

These standard deviations for each month are shown in the top plots of Figures 2.13a and 2.13b for APO and CO_2 respectively. Thus these plots give a statistical measure of the variability in APO and CO_2 at monthly time intervals. To provide a comparison,

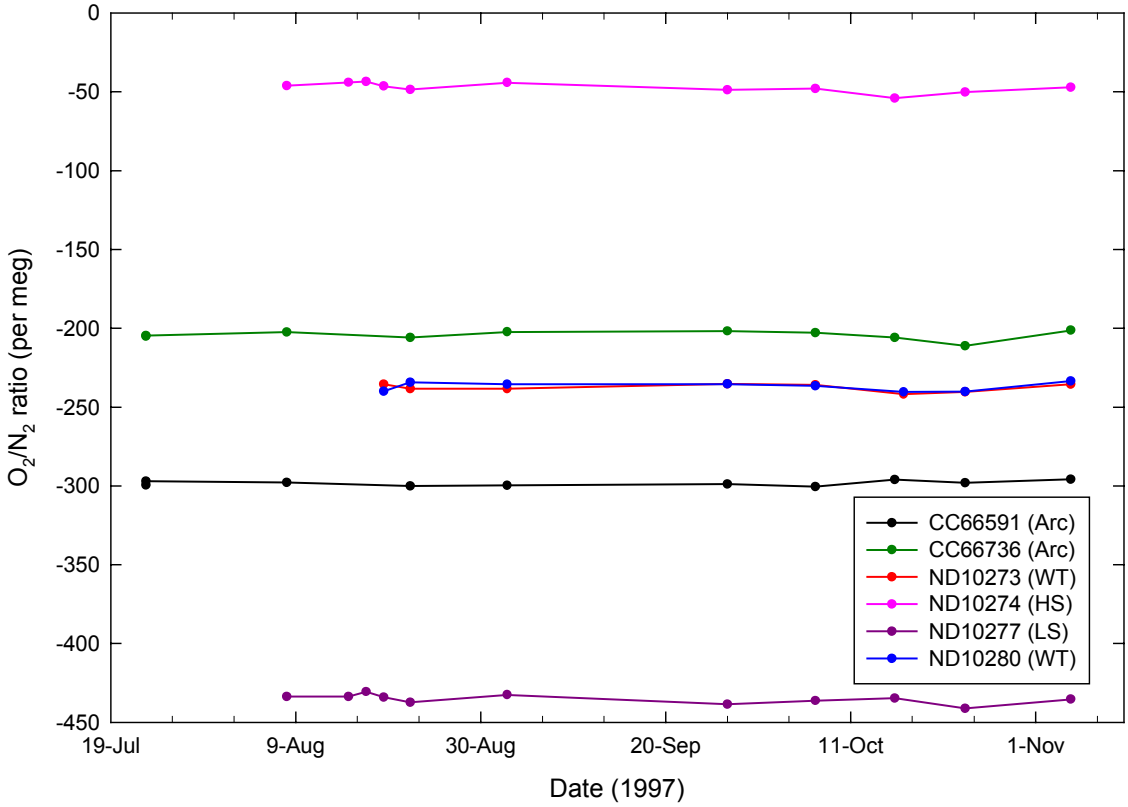

Figure 4.5. Shows the O_2/N_2 ratios calculated on the interferometric analyzer at Scripps of the calibration gases used at Baring Head. "Arc" indicates long-term archive gas cylinders, "WT" indicates working gases, and "HS" and "LS" are high span and low span gases respectively. All gases show good stability in O_2/N_2 ratios over a three to four month period.

(Table 4.1), I can then calculate a daily value for the O_2/N_2 ratio of the working gas. I assign this value for the next 24 hours, until the next HS/LS calibration runs and re-calculates the working gas ratio. Figure 4.6 shows the results of these calculations. Five different working gases have been used in the first 12 months of operation, and these are shown labeled above the data in the figure. Small downward trends are apparent in the working gas concentrations over time. This is probably demonstrating a real change in O_2/N_2 ratio in the cylinders and is most likely owing to decreasing

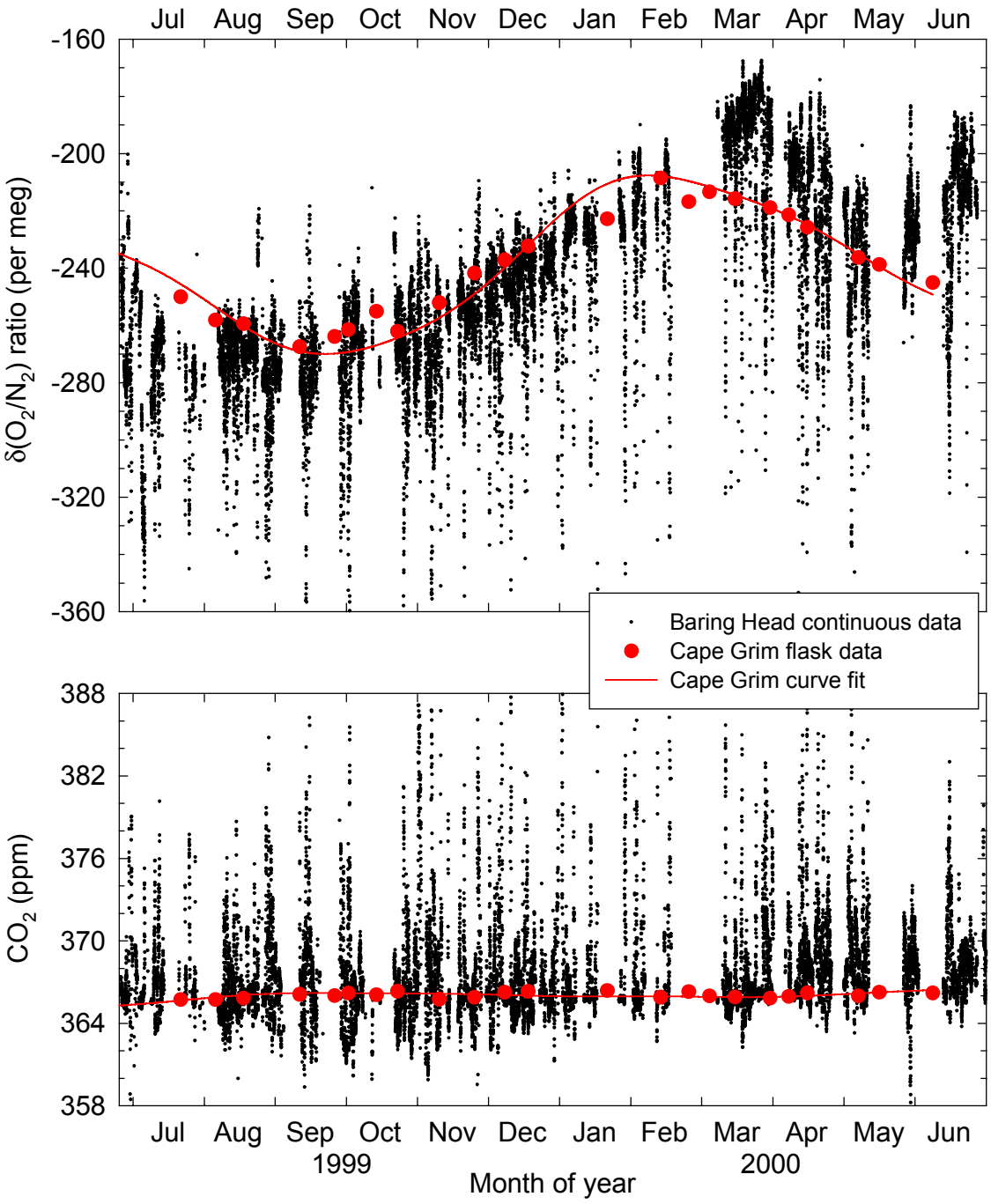

Figure 4.9. Shows all O_2/N_2 ratio and CO_2 concentration data collected at Baring Head from June 1999 to July 2000. Each black data point is an average over 15 minutes. Red data points show flask samples collected at Cape Grim, Tasmania (see Figure 4.1) during clean, background air conditions as a part of the Scripps O_2/N_2 flask sampling network. The red line is a curve fit to the Cape Grim data.

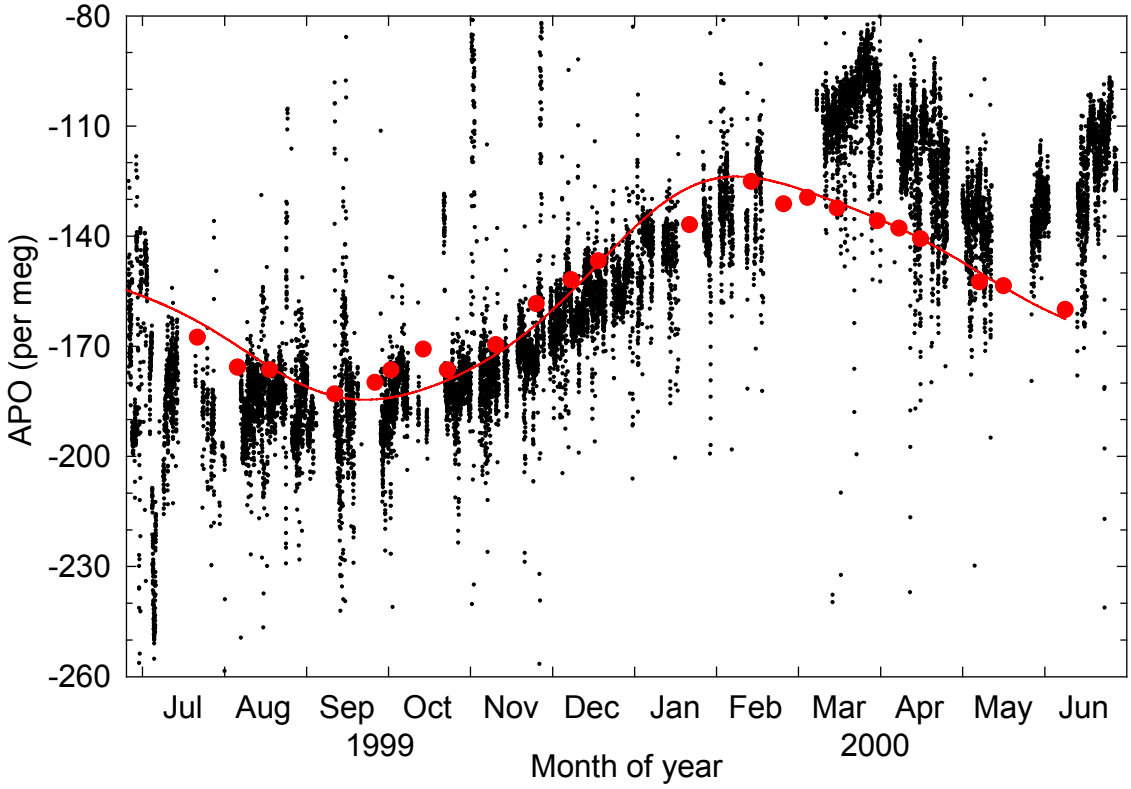

Figure 4.10. Atmospheric Potential Oxygen, APO, at Baring Head from June 1999 to July 2000. This shows the oceanic influence on the air arriving at Baring Head.

Also shown in Figures 4.9 and 4.10, as red symbols, are flasks samples collected at Cape Grim, Tasmania (40.7°S, 144.7°E) as part of our global flask sampling network (Chapter 2). These flask samples are shipped back to our laboratory in La Jolla, California, where they are analyzed for O_2/N_2 ratio on our interferometric analyzer [*Keeling*, 1988] and for CO_2 concentration on a Siemens NDIR analyzer. Curve fits to the Cape Grim data are also shown, consisting of the sum of a four-harmonic seasonal cycle and a stiff spline. The curve fits were calculated from a longer dataset not shown, extending back to 1991.

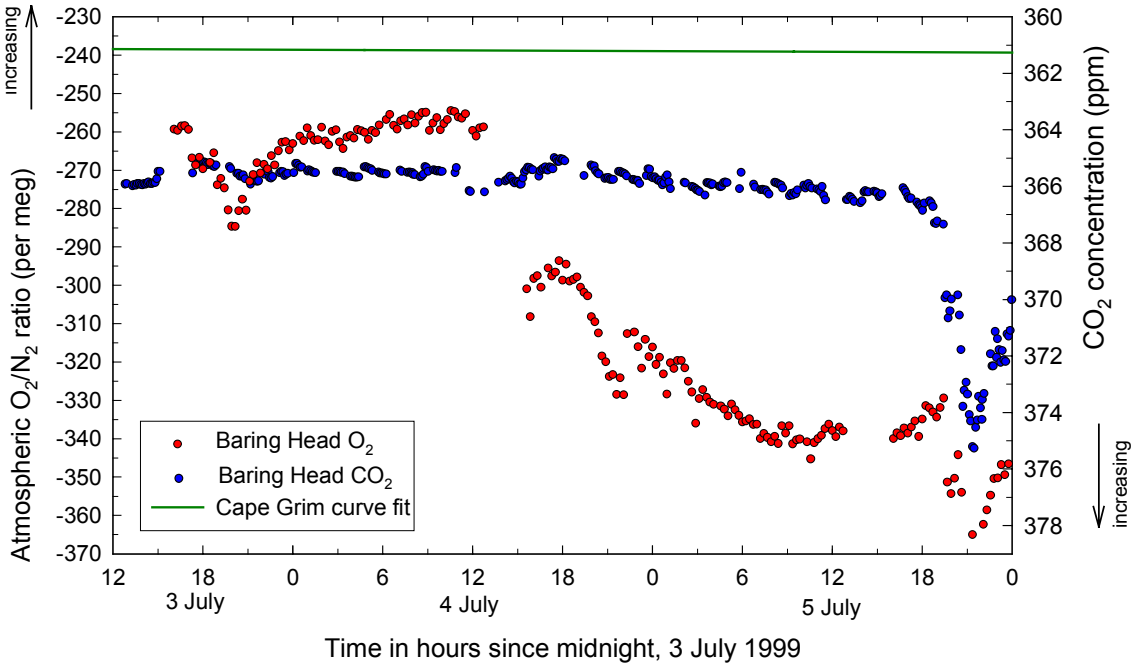

Figure 4.14. O_2/N_2 ratio and CO_2 concentration at Baring Head for 3-5 July 1999. Note that O_2/N_2 ratio and CO_2 concentration axes are reversed with respect to each other. In addition these axes are scaled so that changes in O_2 and CO_2 are comparable on a mole to mole basis. The green line shows the curve fit to the O_2/N_2 ratio data from flask samples collected at Cape Grim, Tasmania.

some technical problems during this time period, as illustrated by the abnormally noisy signal. Therefore a more precise determination on the exact increase in CO_2 concentration can not be made, however, it is clearly of the order of 1.5 ppm.

These changes in O_2/N_2 ratio and CO_2 concentration can not be attributed to land biotic or anthropogenic effects, because the observed O_2:C molar ratio is approximately –11:1, instead of –1.1:1 that would be observed from land biotic effects, or –1.4:1 that would be observed from fossil fuel combustion. This leaves only oceanic processes that could be responsible for the observations.

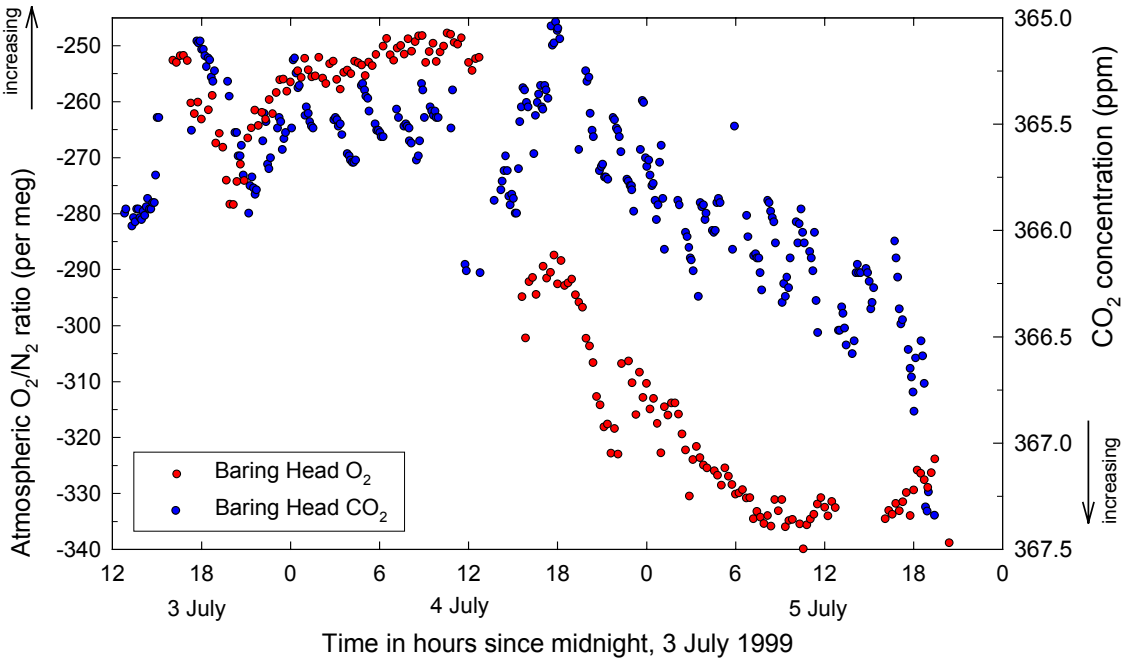

Figure 4.15. As for Figure 4.14, except the CO_2 axis has been blown up, showing that CO_2 concentrations increased at the same time that O_2/N_2 ratios decreased.

To help identify the origin of the sampled air, I have calculated 72-hour backward wind trajectories using the HYbrid Single-Particle Lagrangian Integrated Trajectory model, version 4 (HYSPLIT4), developed by the NOAA Air Resources Laboratory [*Draxler and Hess*, 1998]. This model uses 1° meteorological analyses from the National Center for Environmental Prediction as input fields. In Figure 4.16, I show one such trajectory calculation for air arriving at Baring Head at 12:00, 4 July 1999 NZST. This figure clearly shows that the air arriving at Baring Head was solely of oceanic origin, and from relatively high latitudes in the Southern Ocean.

There is some concern regarding the accuracy of such trajectory models in the southern hemisphere where direct observations are relatively sparse and the model must